Confocal Imaging of 3D Network Structures

Fiona Muir

Department of Physics and Astronomy

University College London

Supervisor: Prof. Ian Robinson

A LEXT Olympus 4000 optical confocal microscope was used to scan through the depth of sections of electrospun PLLA scaffolds and create three dimensional images by using VolumeViewer, a plugin for ImageJ. The method had previously shown a significant drop in contrast through the depth of the sample, with the lower 50% unable to be imaged. Through refractive index matching and the use of a wide range of potential matching media, the full depth of the scaffold was able to be imaged with a small but significantly reduced drop in contrast. The matching media included immersion oil, a number of salt solutions, methyl salicylate and various concentrations of glycerol solution with 91% glycerol solution proving to be the most successful matching medium trialled with 98% of the scaffold depth able to be imaged. This shows promise as a method for imaging cell cultures grown within electrospun PLLA scaffolds and improving future patient treatments.

Contents

1. Introduction

This project focused on using confocal microscopy to image electrospun scaffolds to obtain three dimensional images and finding methods to optimise the images obtained. Refractive index matching of the scaffold was decided to be the most effective and practical way to achieve this and was therefore the method pursued. By saturating areas of the scaffolds with a range of liquids with refractive indices close to that of the scaffold material, it was possible to image deeper into the scaffolds than previously achieved and obtain vital information about their internal structure and basic structural properties. This will be beneficial to current and future projects involving the growth of cell cultures on these scaffolds with possible applications in wound healing, skin grafts and artificial tissue growth.

2. Background Theory

2.1 Confocal Microscopy

Laser scanning confocal microscopy was chosen as a technique for this project for its ability to take "slices" of images through the depth of a sample and create a 3D image by stacking these slices back together. By doing this, it allows the internal structure of scaffolds to be seen in greater clarity and therefore more information was gained about the way cell samples will grow within the scaffolds. This would allow more precise tailoring of usage of scaffolds and therefore more efficient treatments for patients.

Optical confocal microscopy is an imaging technique that differs from traditional microscopy in a number of ways. In traditional wide-field microscopy, the specimen is evenly illuminated throughout. However, in confocal microscopy, each volume element of the sample is illuminated by a point source of light in turn. An objective lens then focuses scattered and reflected light from the sample and it passes through an aperture before the intensity of the transmitted light is recorded by the detector – a photomultiplier tube or avalanche photodiode. By using this technique, only a very narrow depth of focus is obtained. Out of focus light from around the focal plane is prevented from reaching the detector and therefore will show up as black in the images. This means that in essence, only light from a small, in-focus plane of the sample contributes to the each snapshot image. [1] [2] This method of taking multiple images at different focal planes is known as optical sectioning and offers a versatile technique for imaging specimens where areas would otherwise be out of focus or obscured. These snapshot images are then recombined and "stacked" back together to create a three-dimensional representation of the sample. Optical confocal microscopy offers a higher resolution than traditional optical microscopy due to the fact that the minimum contrast required for a distinction to be detected is far lower when using a confocal microscope that it would have been using a nonconfocal imaging

method [3]. A schematic diagram of the basic components of a confocal microscope is shown in Figure 1.

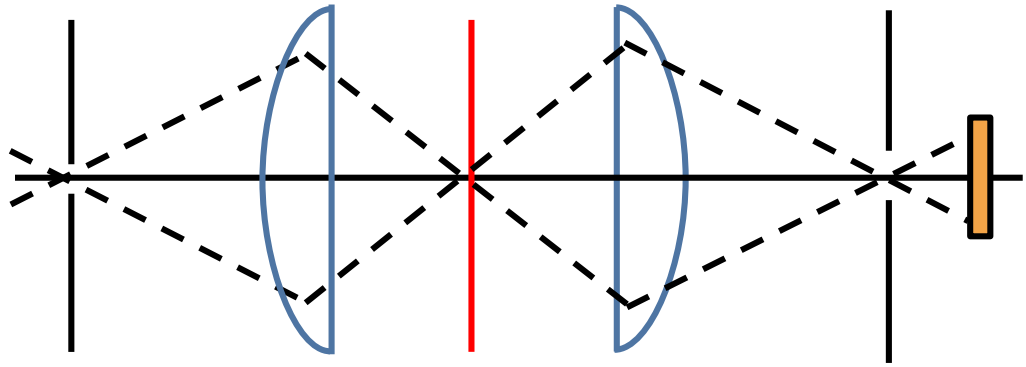

Figure **1** shows a schematic illustration of the layout of a confocal scanning microscope with the red line indicating the plane of focus. The lens is shown in blue and the detector is shown in orange. Either side of the lenses are the focusing apertures and the dashed lines indicate the light rays.

For this project, the microscope used was a LEXT Olympus 4000 3D Laser Measuring Confocal Microscope. It was also able to take nonconfocal images using the LED as a wide field microscopy light source rather than the light source for the confocal imaging and Figure **2** shows the clear difference between confocal (right) and nonconfocal (left) images of the same section of scaffold. In the confocal image, which was focused 5µm below the surface of the scaffold, there is a far higher contrast between fibres and their black background due to surrounding fibres in different focal planes being out of focus and therefore not received as an output when using the confocal technique.

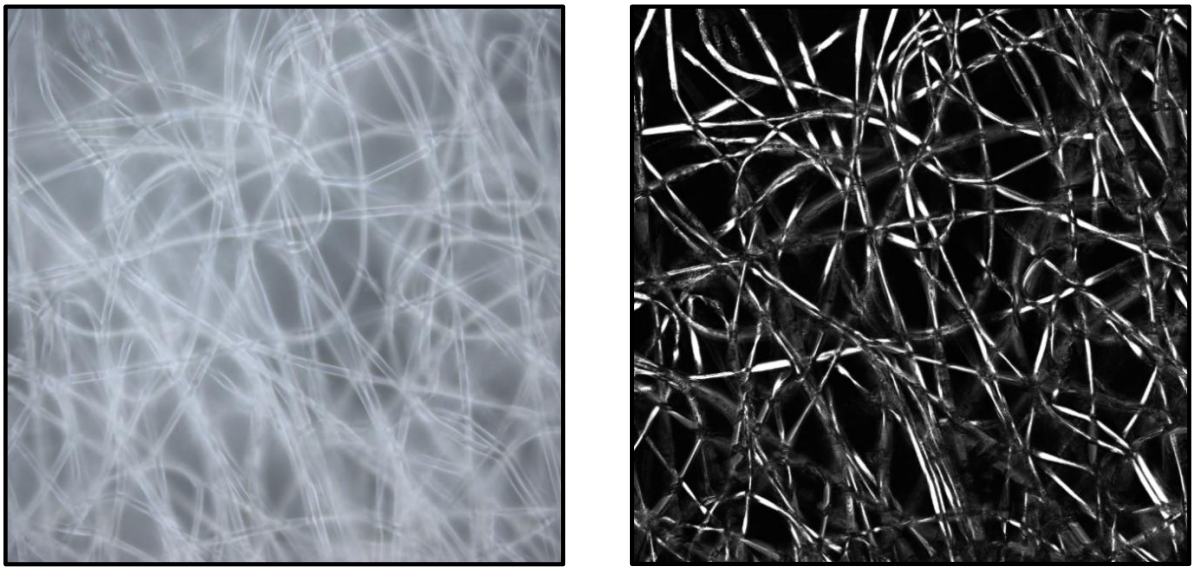

Figure **2** shows nonconfocal and confocal micrographs of the same area of a dry 4µm diameter fibre scaffolds. The confocal image was taken 5µm below the surface of the scaffold and each image shows a 100µm by 100µm square area.

By focusing on a specific focal plane and measuring the vertical position – using the LEXT Olympus software interface – and manually focusing the microscope on different areas, confocal microscopy can

also be used as a method for obtaining depth measurements and mapping the surface of an object. This was used to determine the true depth of the scaffold samples (see section 3.1).

Confocal microscopy has risen to prominence in a range of fields including biomedical applications as it is a practical method for imaging live cell samples and does not need to be performed in a vacuum [2]. It is also a useful technique in semiconductor inspection as the key features of the technique make it ideal for creating 3D images and surface plots of specimens [4]

When creating each image, the light intensity from one illuminated volume element represents one pixel. By taking a slower scan and measuring more points within the plane of interest, the signal to noise ratio is increased, as is the contrast and the resolution of the image. However, this would result in a slower procedure and therefore a longer scan time. The short scan time of small samples and snapshot slice images is one of the key advantages of confocal microscopy over other three dimensional imaging techniques. For example, stereoscopy is the technique of taking optical images from a number of different angles, before combining to create 3-dimensional visualisations of objects. This is a very traditional technique with a number of applications, but in this case it would still require further modifications in order to limit the depth of focus. Ptychography involves creating an image by combing and analysing the diffraction patterns at many positions across a sample [5]. It has been shown to be very effective using X-rays, especially when combined with computed tomography to create a three-dimensional image. It has also been shown to be a practical technique used with optical light [6]. However, ptychography has previously been restricted to samples no more than tens of microns thick. Scanning electron microscopy could have also been a valid technique as it has been gaining prominence as a method for obtaining three dimensional images of biological samples. However, samples must be electrically conducive and totally dry [7]. This both limits options for refractive index matching media but also makes it less suitable for imaging biological samples. Once again, this would be limiting the number of possible applications of the imaging technique and this is not desirable.

2.2 Scaffolds

The samples studied were electrospun polymer scaffolds. These are highly biocompatible structures which can mimic vital features of the extracellular matrix (ECM) – a collection of molecules which surrounds cells providing structural and biochemical support. These scaffolds provide a framework upon which biological samples can be studied and are also able to grow. By growing specimens within the scaffolds, cells are able to maintain their three-dimensional structure thanks to the design of the scaffolds.

Scaffolds have an internal “nest-like” appearance as seen in Figure 2 and a similar thickness to a standard piece of paper (~50µm). They are used in practical biomedical applications including

supporting skin grafts and tissue transplants as they ensure that the cells grow in their natural three dimensional structure and are able to receive necessary biochemical support. As scaffolds are generally porous, they allow nutrients, markers and other biochemical materials to be fed to cell cultures through the matrix of the scaffold, allowing it to mimic even more features of the extracellular matrix.

In this case, the scaffolds used were all made from poly(L-lactide) (PLLA), a specific form of polylactic acid which is a biodegradable thermoplastic aliphatic polyester derived from sugarcane or corn starch. These properties allow would allow for the scaffold to decompose if used as a structure to support a skin graft or tissue replacement, with no need to remove it at a later date. Currently, PLLA is used in a number of biophysical applications, notably temporary implants to aid joint and bone healing. Once again, its ability to biodegrade is vital here as the pins decompose once the injury is healed.

For this experiment, the refractive index of PLLA has been taken to be 1.46, the refractive index of polylactic acid [8]. However this is not exactly the same due to the fact that polylactic acid can refer to a racemic mix of L-lactide and D-lactide rather than heterotactic PLA (which poly(l-lactide) is an example of).

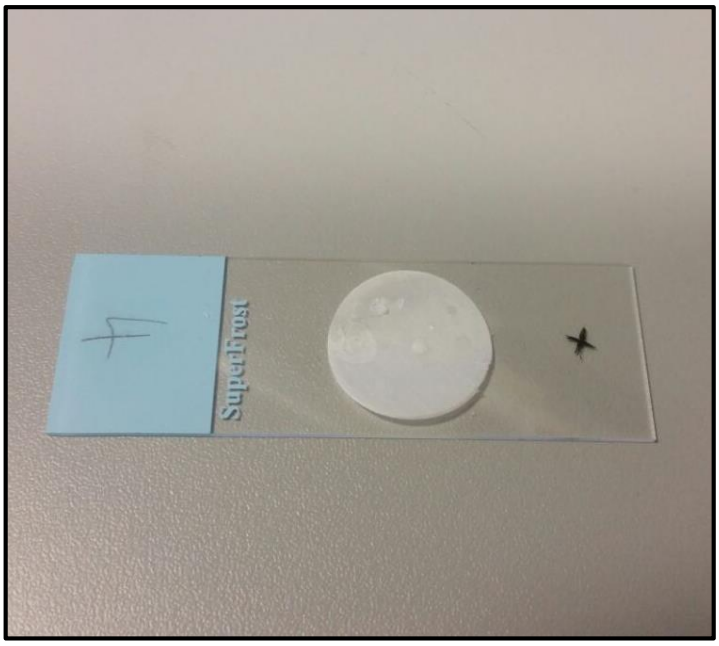

Figure **3** shows a 4µm diameter fibre scaffold on a slide as used for the confocal scans. The raised areas on the surface of the scaffold are salt deposits from the salt solutions which were trialed as refractive index matching media (see sections 3.3.4 and 3.3.7). The cross on the surface of the slide was used to determine the depth of the scaffold (see section 3.1)

2.2.1 Electrospinning

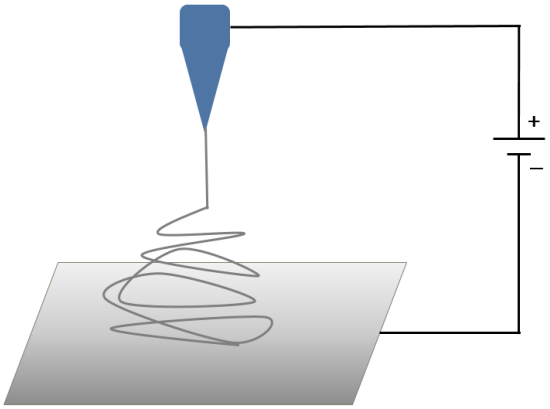

Figure **4** shows a schematic diagram of the process of electrospinning, including the collecting plate and nozzle with a potential difference between them and the fibres from the tip of the nozzle.

The scaffolds for this experiment were produced through a method called electrospinning. Electrospinning uses an electric charge to produce very fine fibres from a molten liquid sample. The liquid is injected through a highly charged nozzle and a charge is induced on the surface of the droplet of liquid. The surface tension of the droplet is overcome when the charge between the liquid and the oppositely charged collecting plate becomes sufficiently high and at this point the liquid is drawn towards the collecting plate. This is a similar method to electrospraying materials in droplets. However, with stronger materials such as polymers and ceramics and by carefully setting the parameters of voltage and the distance between the tip of the nozzle and the collecting plate, fibres are able to be formed [9]. It is also possible to produce different diameters of fibres by varying the voltage and distance from the nozzle to the collecting plate. The Electrospinning Company, which produced the scaffolds for this investigation, produce 1µm, 2µm and 4µm fibre diameter PLLA scaffolds and for each of the refractive index matching media, they were trialled on both the 1µm and 4µm fibre scaffolds. Varying diameters of fibres would be used for different biomedical applications and this was to ensure that the imaging techniques found would be as versatile as possible.

2.2.2 Current Applications

There are a huge number of possible applications for scaffolds and they are currently in use in a variety of projects, including those focusing on bone regeneration and cardiac tissue engineering [10]. In “Porous scaffold design for tissue engineering”, Hollister describes the shift that is occurring in the field of tissue engineering, towards a focus on electrospun scaffolds made from more biocompatible materials, rather than synthetic implants and tissue grafts [11]. Scaffolds have helped to engineer a huge breakthrough in tissue replacements and skin grafts by speeding up cell growth, improving the

structure of the cells grown and improving the bonds from damaged skin to the new skin cells [12]. More recently, there has been successful work on growing muscle tissue on electrospun scaffolds and there is potential to combine scaffolds with inkjet printing of cells on to the structures [13]. This would mean that the structure of the cell cultures would closely mimic the distribution of complex organic tissues, including neurones. It is clear that effective three dimensional imaging of scaffolds and more knowledge of their internal structure would be beneficial to the work being carried out at the moment and could shed light on the behaviour of cells within the scaffolds.

3. Method

3.1 Microscopy

In order to confirm the true depth of the scaffolds, a feature of the LEXT Olympus software was used. By focusing the microscope on a point on the surface of the slide then manually adjusting the microscope to focus on a point on the top surface of the scaffold, it is possible to gain an approximate value for the thickness of the scaffold. By performing the measurement at a large number of points on the surface of the scaffold in a range of locations, the depth was confirmed to be (50±4)µm. This corresponded with the reported value for the thickness from The Electrospinning Company and was used to confirm that the short internal depth which the confocal microscope could image was due to a marked decrease in contrast rather than reaching the bottom of the scaffold.

To examine the potential of confocal microscopy as a method for imaging, an initial scan of a dry scaffold was carried out for both the 4µm diameter fibre and 1µm diameter fibre scaffolds. The scan began at the very top surface of the scaffold and snapshots were taken every 0.25µm through the scaffold until the output was totally black or the contrast was so low that no individual fibre could be identified. A series of some of the initial snapshots can be seen below. It was possible to see the internal structure of the scaffolds clearly at first and it is possible to see in the later images that the contrast decreases to the point that images taken of cell cultures would not be able to offer any valuable information. This corresponded with the initial aims of the project and gave a starting point for the refractive index matching technique to improve upon. In this initial scan, it was possible to image the top 22.50µm or 45% of the reported depth of the scaffold.

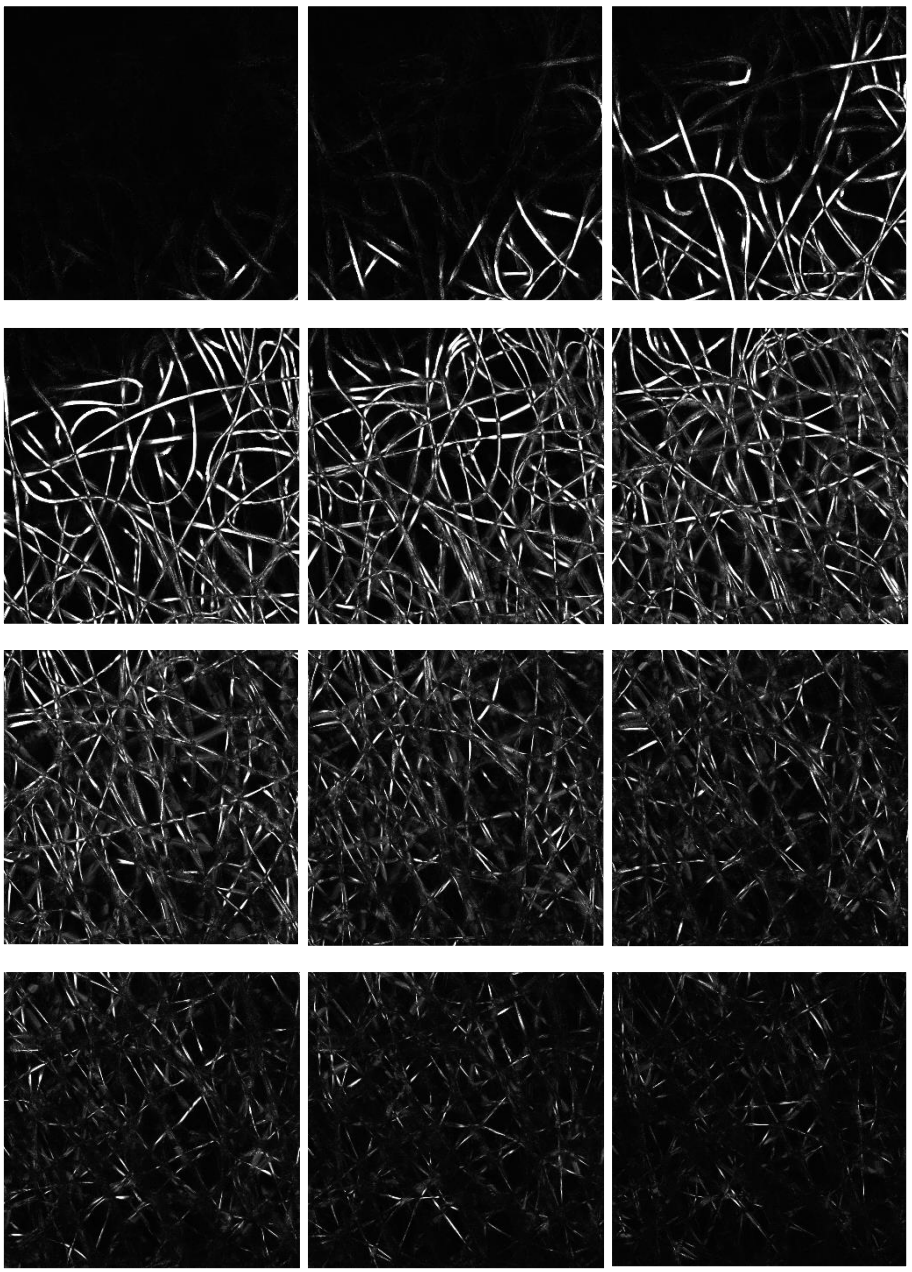

Figure **5** shows a series of 12 images taken through the dry 4µm fibre scaffold. They are taken in steps of 1.75µm and show a combined depth of 21µm. The top left image shows the top surface and they continue left to right and top to bottom. It is clear to see that there is a distinct drop in contrast even within the first 21µm

This same procedure was repeated for all the refractive index matching media with the images either being taken at steps of 0.25µm (for 50x magnification) or 0.8µm (for 20x magnification). In general, the lower magnification was used when the matching medium created some kind of effect or feature on the scaffold that was not clearly visible at 50x magnification (see section 3.3.7, for example). Snapshot images of the slices of the scaffolds took approximately five seconds to be processed with a full scan taking between 20 and 30 minutes depending on the size of steps taken through the depth and the magnification.

3.1.1 Image Judgement, Uncertainty and Determining Depth

The project is undeniably subjective and there was some personal judgement involved in determining when the fibres in the image were "visible" or "not visible". In order to make this as consistent and quantifiable as possible, the starting point at the top of the scaffold was taken to be the point at which the first sight of non-black pixels were seen and the bottom point – where the contrast was so low as to make the images unusable – was taken to be the last image where an individual fibre could be identified. By looking at the range of images around these endpoints for a variety of different scaffolds and matching media, it was possible to estimate that there was an error of two images either side of the image chosen. Therefore, the uncertainty of the start and end points has been taken as twice the depth step used in that scan (either ±0.5µm or ±1.6µm).

When using automatic stacking scripts which adjusted the focal depth and performed the scans, it was found that they automatically adjusted the brightness and contrast in order to obtain the best possible quality of image. However, for this project that was not desirable as it meant that it was impossible to see a decrease in contrast due to the confocal microscope as it would be masked by increases in brightness and contrast performed by the software. Therefore, each of these scans was performed manually, taking snapshot images and moving the focal depth by the smallest possible step using the LEXT Olympus software user interface in between pictures.

Shown below are a two series of images, each taken in steps of 0.25µm, illustrating what was taken as the top surface and what was taken as the last visible image in a scaffold sample.

Figure **6** shows a series of pictures of the top surface of the scaffold to indicate which would be taken in to account in this experiment.

In this series, the typical top surface of a scaffold is shown. The image on the left would not be included as it is too dark, the middle image would possibly be included and is uncertain. The image on the right would be included as it is possible to see the top surface of the fibres.

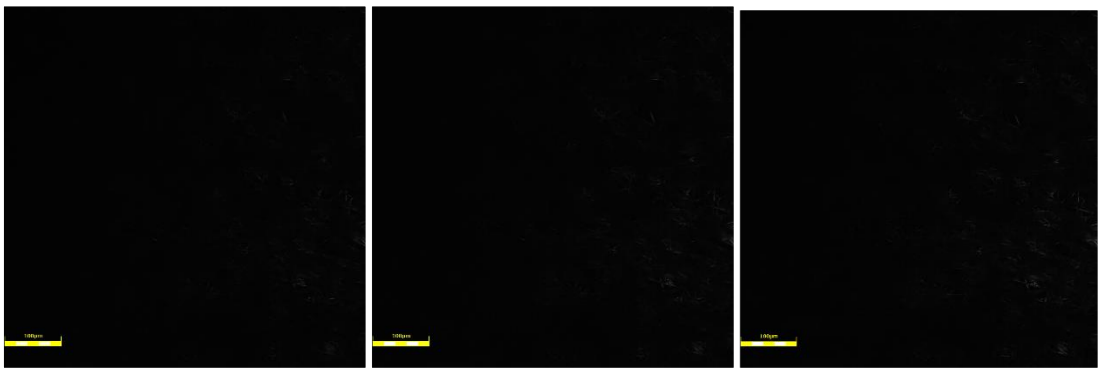

Figure **7** shows a series of images which could be taken as the last possible visible image in an image stack within a scaffold.

In this series, the typical fade to darkness within a scaffold is shown. The image on the left would not be included as it is too dark, the middle image would possibly be included and is uncertain. The image on the right would be included as it is possible to see individual fibres.

3.1.2 Apparent Depth

Apparent depth is an optical phenomenon which causes the depth of objects which have a refractive index higher than air to appear shorter than it actually is by a factor of the refractive index. Therefore, the bottom surface of the scaffold should be appear to be at a depth of:

$$\frac{50\mu m}{n_{matching\ medium}}$$

With purified water for example, it would be expected for the scaffold depth to be reduced by a factor of 1.33 compared to the dry scaffold and for the maximum depth able to be imaged to be 37.5µm.

3.3 Refractive Index Matching

Once the actual thickness had been confirmed and an initial imaging depth was obtained, methods were explored to improve the depth to which the confocal microscope was able to image within the scaffolds. The key method employed was refractive index matching. This involves replacing the air in between the fibres and filling the porous gaps in the fibres of the scaffold with a fluid with refractive in between that of the scaffold (n=1.46) and air (n~1.00) [14].

In the case of using a fluid with an identical refractive to the scaffolds' refractive index, there would be no reflection or refraction of light crossing over the boundary and this would offer no benefits in terms of imaging the fibres. The boundary would be effectively invisible and would make effective imaging impossible. In the case of approximately equal refractive indices, it would greatly reduce the light reflected and refracted and increase the optical clarity of the sample. This phenomenon can be shown by inspecting the Fresnel equations for transmitted and reflected light between media boundaries.

$$t_{\perp} = \frac{2n_1 \cos\theta_i}{n_1 \cos\theta_i + n_2 \cos\theta_t} \quad (1)$$

$$r_{\perp} = \frac{n_1 \cos\theta_i - n_2 \cos\theta_t}{n_1 \cos\theta_i + n_2 \cos\theta_t} \quad (2)$$

As the light from the confocal microscope is incidental on the surface perpendicularly, $\theta_i = \theta_t = 0$ and$\cos\theta_i = \cos\theta_t = 1$.

Therefore, the Fresnel equations become:

$$t_{\perp} = \frac{2n_1}{n_1 + n_2} \quad (3)$$

$$r_{\perp} = \frac{n_1 - n_2}{n_1 + n_2} \quad (4)$$

From this it can be seen that as $n_1 \rightarrow n_2$, $t_{\perp} \rightarrow 1$ and $r_{\perp} \rightarrow 0$. Therefore, the closer that n_1 is to n_2, the more light is transmitted and the less that is reflected. This light is then reflected back through air to the detector of the confocal microscope In order for index matching to be an effective technique, the refractive index of the sample and that of the solution surrounding it must be close but not exactly equal. For this reason, the fluids investigated generally had an intrinsic refractive index close to that of the scaffold or were in solution and by changing the concentration of the solution, the refractive index could be varied. The solutions offered greater flexibility of refractive index. However, they also presented limitations in terms of decreased accuracy of refractive index and, in some cases, limited permeation of the fluids in to the scaffolds.

Refractive index matching is a common method used with immersion microscopes and lenses, usually using lens oil, purified water or, more recently, glycerol. Therefore, the first fluids trialled were immersion oil and purified water.

Over the course of the experiment, ten individual fluids were used as possible refractive index matching media:

Refractive index matching medium	Refractive index, n
Immersion oil	1.518
Purified water	1.333 [15]
20% by mass sucrose solution	1.364 [16]
Ethanol	1.361 [15]
20% by volume ethanol solution	1.346 [17]
0.1M Potassium Iodide solution	1.336 [18]

4M Caesium Chloride solution	1.380 [18]
55% Glycerol solution	1.406 [19]
91% Glycerol solution	1.460 [19]
Methyl Salicylate	1.535 [20]

Table 1 shows the refractive indices of the potential matching media used within the experiment.

3.3.1 Immersion Oil

When imaging the immersion oil soaked scaffolds, some of the colours in the images were inverted (as seen below in Figure 8). Rather than the fibres appearing light and the rest of the image dark, the fibres appeared dark and the gaps between them appeared bright. In the 4µm diameter fibre scaffolds, the centres of the fibres appeared white and the edges were dark, with the oil appeared white once again. This could seem to indicate that the oil was no able to fully permeate in to the thicker fibres. Upon further investigation, the refractive index of the oil (n=1.518) did not lie between the refractive index of air and the refractive index of the scaffold. Therefore, it was not the most suitable liquid to use for this investigation. It did improve the imaging depth to some extent but the inverting of the colours can be attributed to the high relative refractive index compared to the poly(L-lactide). It was possible to image to a depth of 27.25µm in the 1µm fibre scaffold and 27.50µm in the 4µm fibre scaffold.

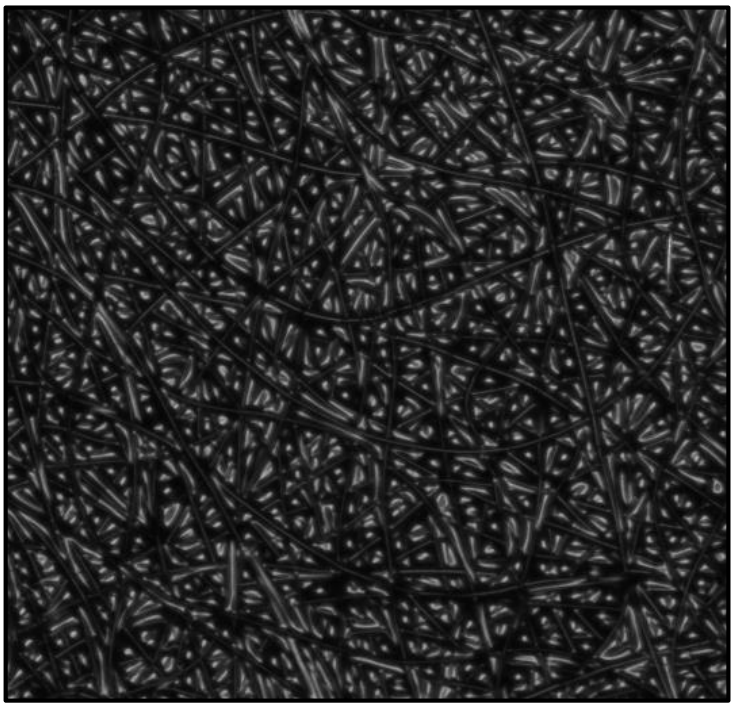

Figure **8** shows a 20x magnification confocal image of the 4µm diameter scaffold soaked in immersion oil.

3.3.2 Purified Water

Areas of the scaffold were then saturated with purified water (n=1.333). This was used because the refractive index lies in between that of the scaffolds and that of air. However, this was not close to the refractive index of the scaffold and was not expected to perform well. In practice, the water gave a crisp image as it was able to permeate in to the scaffolds well but as the refractive index was not that close to that of PLLA, the imaging depth was not hugely improved and it was possible to image to a depth of 28.75µm in the 1µm fibre scaffold and 35.75µm in the 4µm fibre scaffold.

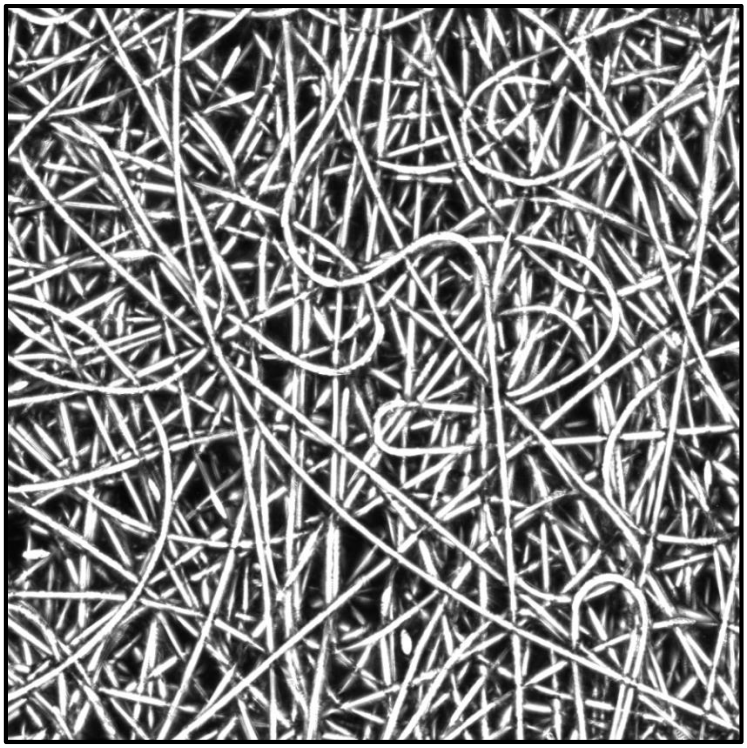

Figure **9** shows a 20x magnification confocal image of the 4µm diameter scaffold soaked in purified water.

3.3.3 Sucrose Solution

The next solution trialled was various concentrations of sucrose solution. However, the solutions were too viscous and did not permeate in to the scaffold. Figure **10** shows the edge of the drop of 20% sucrose solution on the surface of the scaffold. It can be seen that the sucrose solution is remaining sitting in the gaps between the fibres and is not allowing the individual fibres themselves to be imaged. This created a lensing effect on the top surface and distorted the images below and optical sectioning could not be used effectively. The sucrose solution scattered a large amount of the light and did not make for a useful refractive index matching medium.

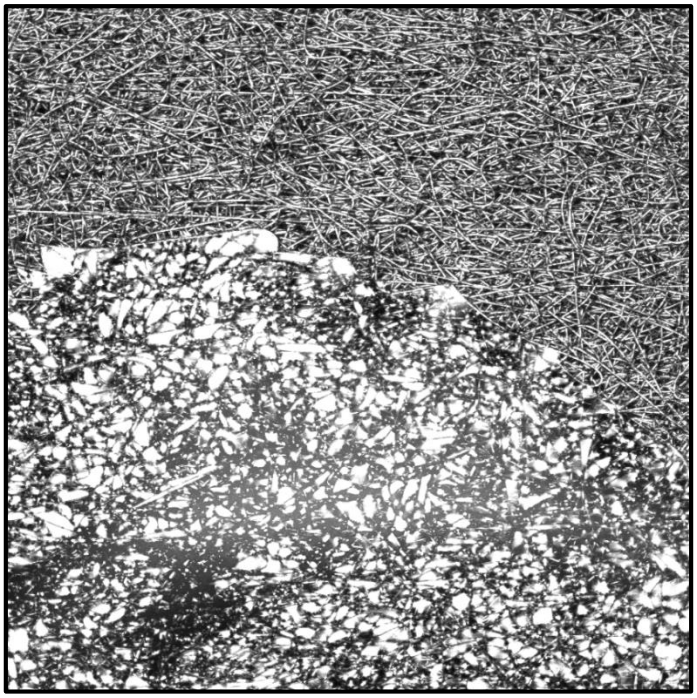

Figure **10** shows a 10x magnification image of the drop of sucrose solution on the 1µm fibre scaffold after being left to permeate for 48 hours. The sucrose solution is at the bottom of the image with the dry scaffold visible in the top half

3.3.4 Caesium Chloride Solution

In the case of 4M Caesium Chloride solution, the water appeared to permeate in to the scaffold, leaving an area of salt crystallised on the top surface of the scaffold (see Figure **11**).

Figure **11** shows a 5x magnification confocal image of the crystal of caesium chloride salt solution on the surface of the 1µm fibre scaffold. Examples of the dark areas of interest can be seen highlighted in red.

This appeared to be unsuitable for confocal microscopy and to be impossible to image. However, closer inspection revealed that around the main area of salt deposits, there was a band which was not fully obscured by the salt crystal in between the crystal and the dry scaffold.

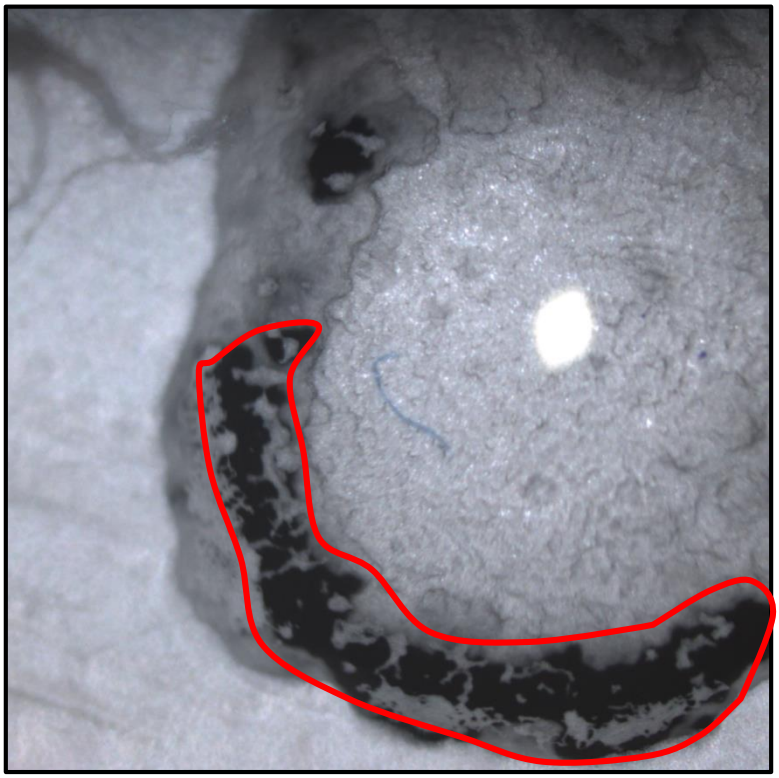

Figure **12** shows a 5x magnification nonconfocal image of the caesium chloride salt crystals on the 1µm fibre scaffolds with the dark region of interest clearly visible at the bottom of the image

In nonconfocal images, the area appeared black but it was unclear whether it was totally opaque or transparent. This is shown in Figure **11** and **12** as the areas highlighted in red. When viewed using the confocal laser microscope, it became clear that the areas of scaffold around the salt had indeed become saturated and were able to be imaged. They appeared to have a higher contrast than the dry scaffold surrounding it. This yielded an imaging depth of 41.5µm.

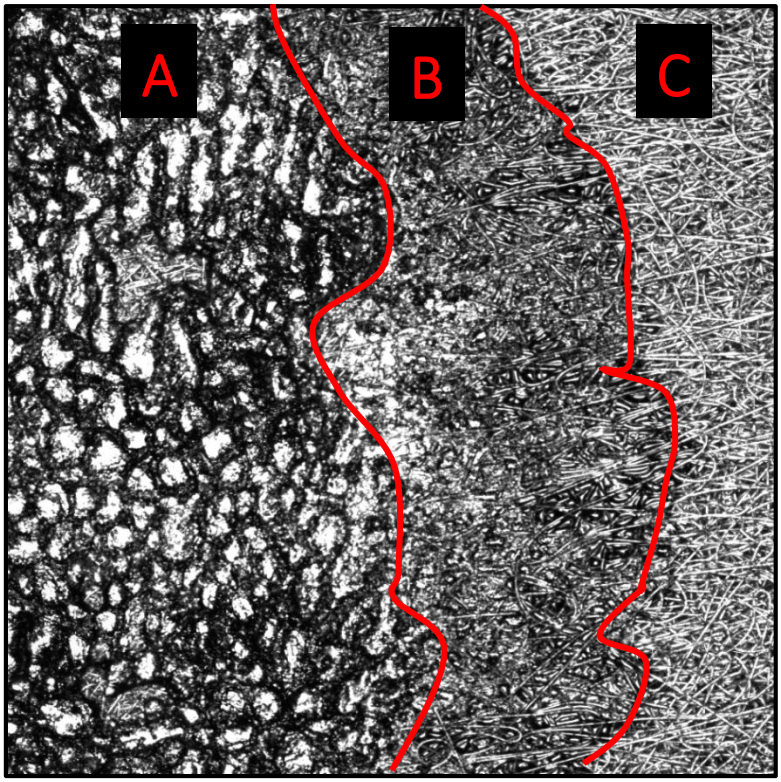

Figure **13** shows a 10x magnification image of the 4µm fibre scaffold showing the three distinct regions which appeared in the caesium chloride soaked scaffold. Region A shows the caesium chloride crystals on the surface, region C shows the dry scaffold and region B shows the high contrast area of interest which was able to be imaged effectively.

3.3.5 Ethanol and Ethanol Solution

Ethanol (C_2H_6O) has a refractive index in the desired range and is a commonly available substance when working with cell cultures. It would therefore make a practical refractive index matching medium if it was found to improve imaging depth. However, ethanol was found to be an unsuitable choice as it had a large effect on the structure and internal architecture of the scaffolds. When 3µl of 100% ethanol was applied to the scaffold, the fibres were seen to align themselves with one another and lie flush against each other, rather than remaining in the nest like structure previously seen. Figure **14** compares an area of a 4µm diameter scaffold with the same area 10 minutes after 100% ethanol had been applied to the area.

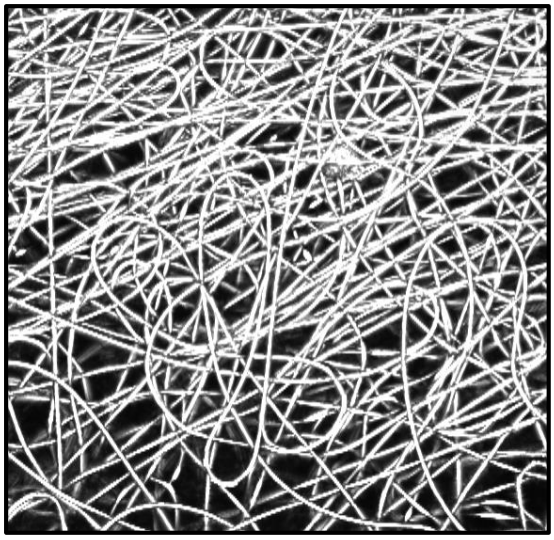

Figure **14a** shows a single focal plane slice image of the 4µm fibre scaffold with 20x magnification. Figure **14b** shows the same area 10 minutes after 3µl of 100% ethanol had been applied to it.

The same effect was seen with 20% by volume ethanol solution and this would clearly make ethanol unsuitable for use with cell cultures as it has too large an effect on the structure of the scaffolds. This in turn would cause cells grown within the scaffolds to have a non-uniform and unnatural structure, making the imaging technique ineffective no matter the depth imaged to.

3.3.6 Glycerol Solution

When investigating glycerol ($C_3H_8O_3$) solution as a possible index matching medium, two different concentrations of solution were mixed up. Firstly, 91% glycerol was used as this has a refractive index of 1.460, very close to the value of the refractive index for PLLA. In order to combat potential issues with too high a viscosity – as seen in the sucrose solution – 55% glycerol solution was also trialled. This has a refractive index of 1.406 but a much lower viscosity. Initially, both concentrations of glycerol solution did not absorb fully in to the scaffold. However, after leaving the samples for one week, both concentrations had absorbed in to the 4µm fibre scaffolds. The 91% glycerol solution was however too viscous to permeate in to the denser 1µm fibre scaffolds. Initially, this did not look like a viable method of imaging as the very top layer of the scaffold can be seen to have 'bubbles' of glycerol caught between fibres, not absorbed in to the scaffold. However, this top layer of glycerol was around 1µm thick and by using optical sectioning, it was possible to image the rest of the scaffold below which has been fully soaked with the glycerol solution. This gave very good results as it was possible to image to 48.8µm in the 4µm fibre scaffolds using the 91% glycerol solution.

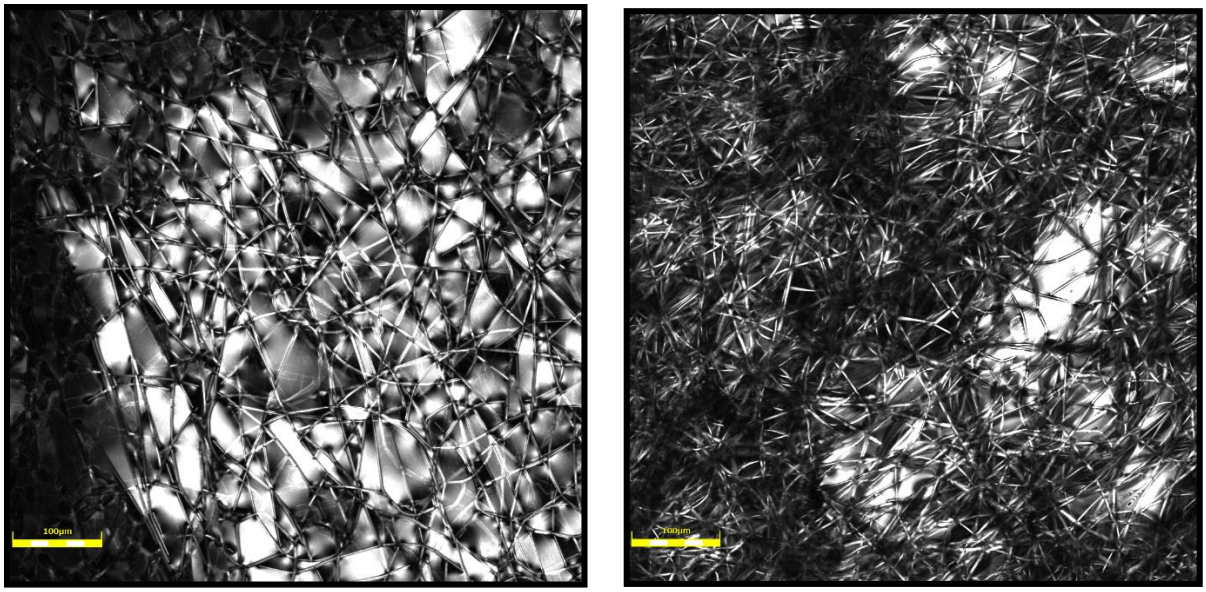

Figure **15a** shows a 20x magnification image of the top surface of a glycerol soaked 4µm fibre scaffold after being left for a week and Figure **15b** shows the midpoint of the same scaffold, using optical sectioning to image below the surface.

3.3.7 Potassium Iodide Solution

The second salt solution trialled was potassium iodide solution and at first, there appeared to be the same issues with salt crystallisation on the surface as with caesium chloride solution. However, while there were salt crystals present on the top surface they were much smaller and dispersed further than the one large area of caesium chloride residue.

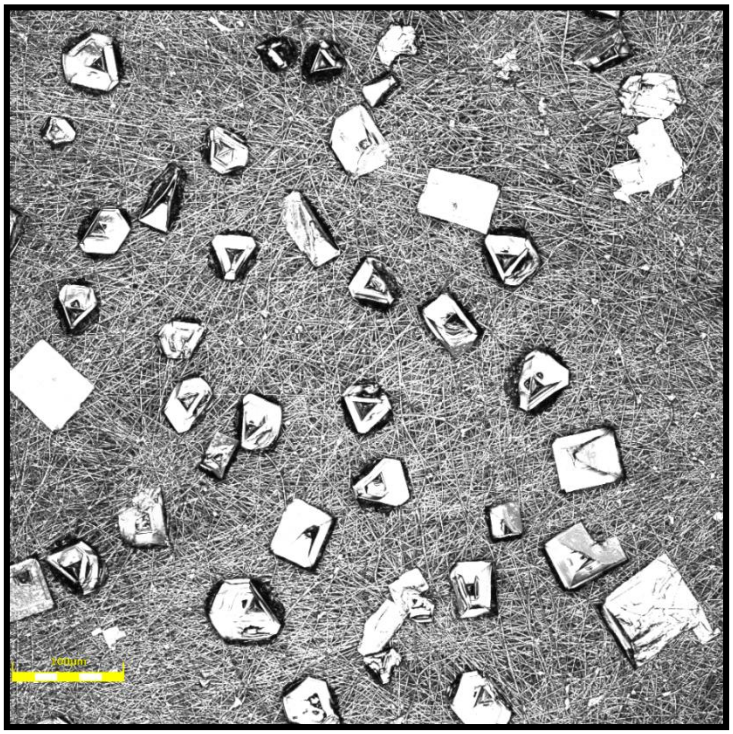

Figure **16** shows a 10x magnification images of the surface of the 1µm fibre scaffold soaked in 0.1M potassium chloride solution. Individual potassium chloride salt crystals are clearly visible on the top surface of the scaffold.

The areas in between the crystals were able to be imaged to a depth of 23.75µm in the 1µm scaffold and 28.00µm in the 4µm fibre scaffolds. However, in a typical region, 25% of the surface was covered by crystals and unable to be imaged. This would be a significant loss in information for imaging the scaffold samples.

3.3.8 Methyl Salicylate

Methyl Salicylate ($C_8H_8O_3$, also known as Methyl 2-hydroxybenzoate) – a synthesised version of wintergreen oil, found in a range of plant species – is often used as a clearing agent in tissue samples, including for use in confocal microscopy. Futhermore, there have been reports that it improves the optical clarity and imaging of samples, regardless of pigment clearing [21]. However, as seen in Figure 17, the methyl salicylate reacted with the PLLA to totally destroy the internal structure of the scaffolds. When viewed under the confocal microscope ten minutes after pipetting 1µl on to the 1µm fibre scaffold, no individual fibres could be seen:

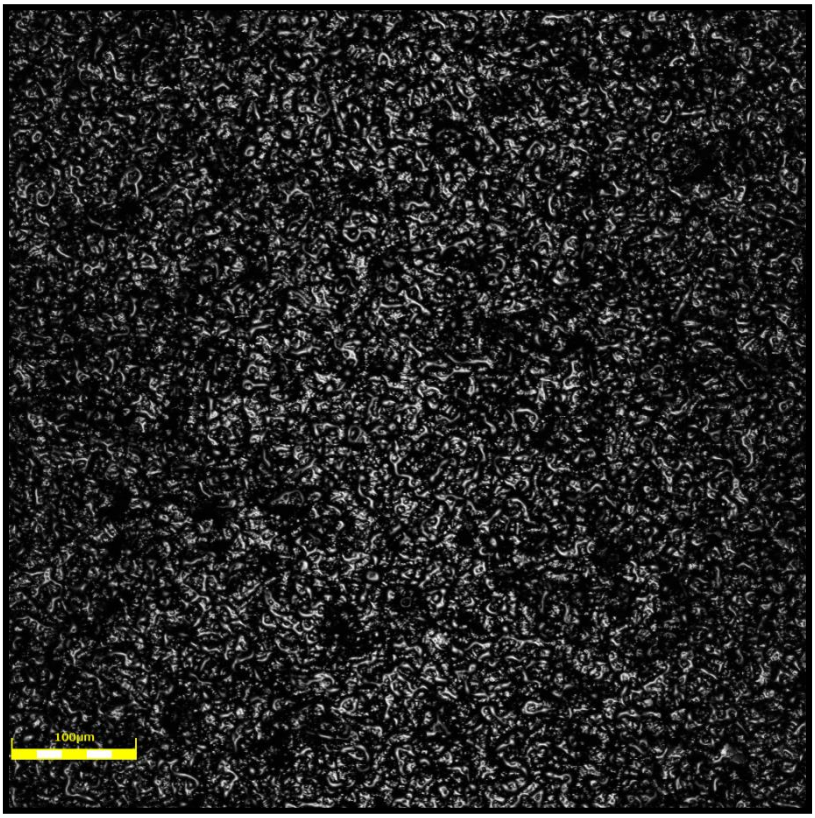

Figure **17** shows a 20x magnification image of the 1µm fibre scaffold ten minutes after soaking the area in methyl salicylate. The internal "nest-like" structure is no longer present.

Figures **18a** and **18b** show the same 1µm fibre scaffold ten minutes after being soaked with 1µl of methyl salicylate and 48 hours after being soaked in methyl salicylate.

As seen in Figures 18a and 18b, the methyl salicylate caused irreparable damage to the scaffolds and was not suitable for use with the PLLA scaffolds.

3.4 ImageJ and Image Analysis

The images obtained in each case where a full scan was possible were "stacked" together to create 3D images using ImageJ, a piece of NIH software [22]. These 3D images can yield both important information about the internal structure of the scaffolds and show clearly how the images fade and deteriorate through the depth of the scaffolds. In all cases, it became apparent that the fibres tend to lie parallel to the plane of the scaffold, rather than having a random orientation. This could provide important information for growing cell culture on the scaffolds.

The three dimensional visualisations were created using the VolumeViewer plugin for ImageJ. Once dimensional variables had been input, the program created a visualisation of a small square sample of the scaffold (as seen below).

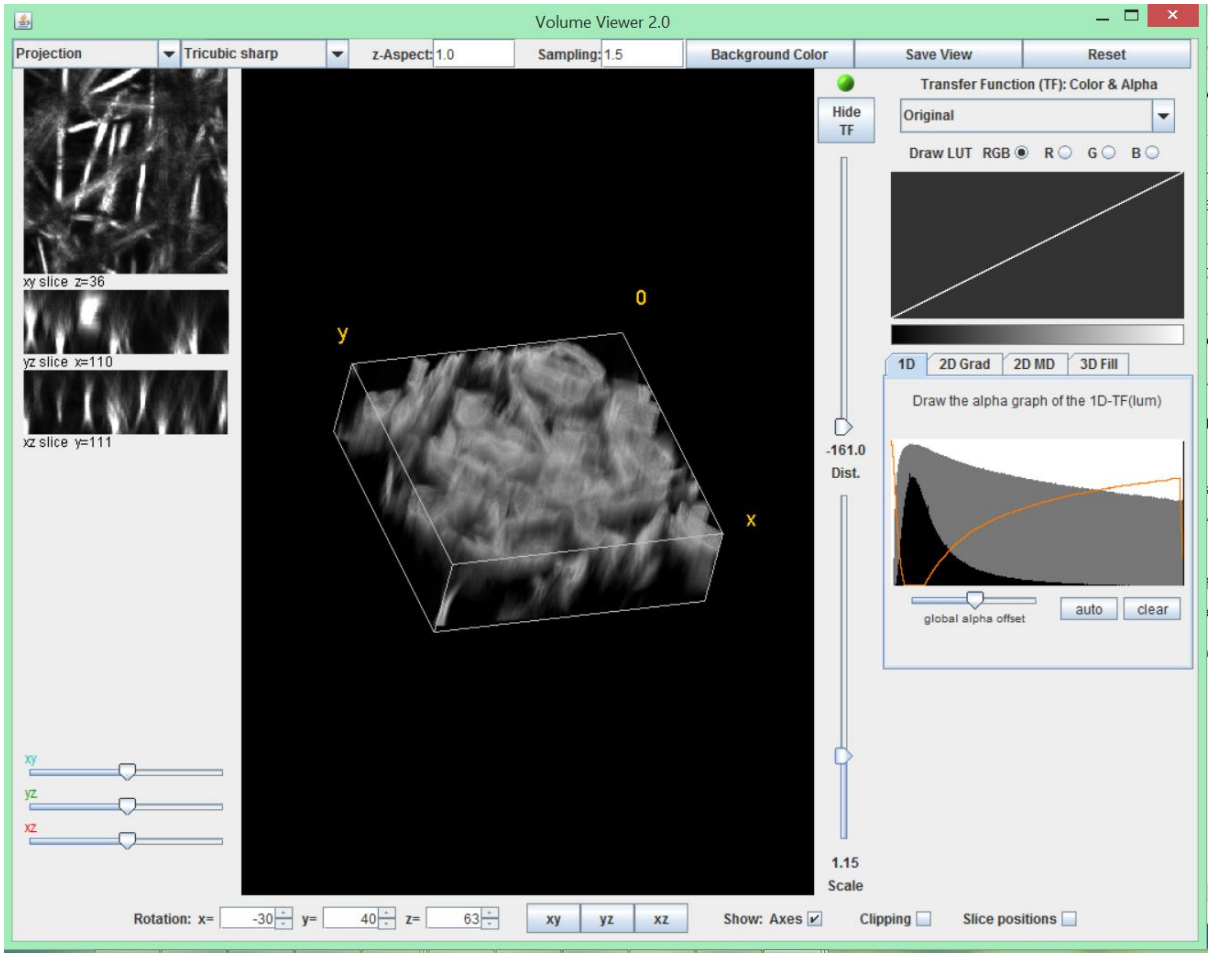

Figure **19** shows the user interface of the ImageJ plugin VolumeViewer. Shown in the centre is a section of dry scaffold imaged in preliminary investigations.

ImageJ allows the three dimensional sections to be rotated and "sliced" through to find cross-sections at any point. This made it a versatile technique which gave much more immediate, easy to interpret information than the raw image stack itself.

3.4.1 Intensity Measurements

By using the ImageJ function "Plot Z-axis Profile", it is possible to obtain a measurement of how intensity varies through the stack of images. This is useful to see how the image fades away due to the fact that, as brightness and contrast have been kept as constant, the intensity is a fair representation of image quality.

The intensity profile is created by assigning each pixel a value of intensity between 1 (black) and 255 (white). The mean for the image slice is then calculated and taken as the intensity for that particular image. It is the mean intensity for each slice which is plotted here in Figures 22 and 23.

4. Results

4.1 Imaging Depth

The tables below show the full scanning depth that was able to be achieved with each of the refractive index matching media. There seems to be no overriding trend to the relation between the imaging depts. In the 1µm and 4µm scaffolds. They both follow the same general trends when it comes to imaging depth being improved by each fluid, however, there is no consistency to whether the 4µm or 1µm scaffold is imaged to a greater depth for each fluid. This could be a topic to investigate further as while it seems that there is no impact, they are not similar enough environments for them to be assumed to behave in the same manner for each of the fluids.

4.1.1 1µm Diameter Fibres Scaffold

Liquid	Depth imaged (µm)
None – dry scaffold	24.75
Immersion Oil	27.25
Purified Water	37.50
Caesium Chloride Solution	-
55% Glycerol Solution	40.50
91% Glycerol Solution	-
Potassium Iodide Solution	36.00

Table **2** shows the depth imaged to within the 1µm fibre diameter scaffold

4.1.2.4µm Diameter Fibres Scaffold

Liquid	Depth imaged (µm)
None – dry scaffold	22.50
Immersion Oil	27.50
Purified Water	35.75
Caesium Chloride Solution	41.50
55% Glycerol Solution	48.80
91% Glycerol Solution	48.00
Potassium Iodide Solution	29.75

Table **3** shows the depth imaged to within the 4µm fibre diameter scaffold

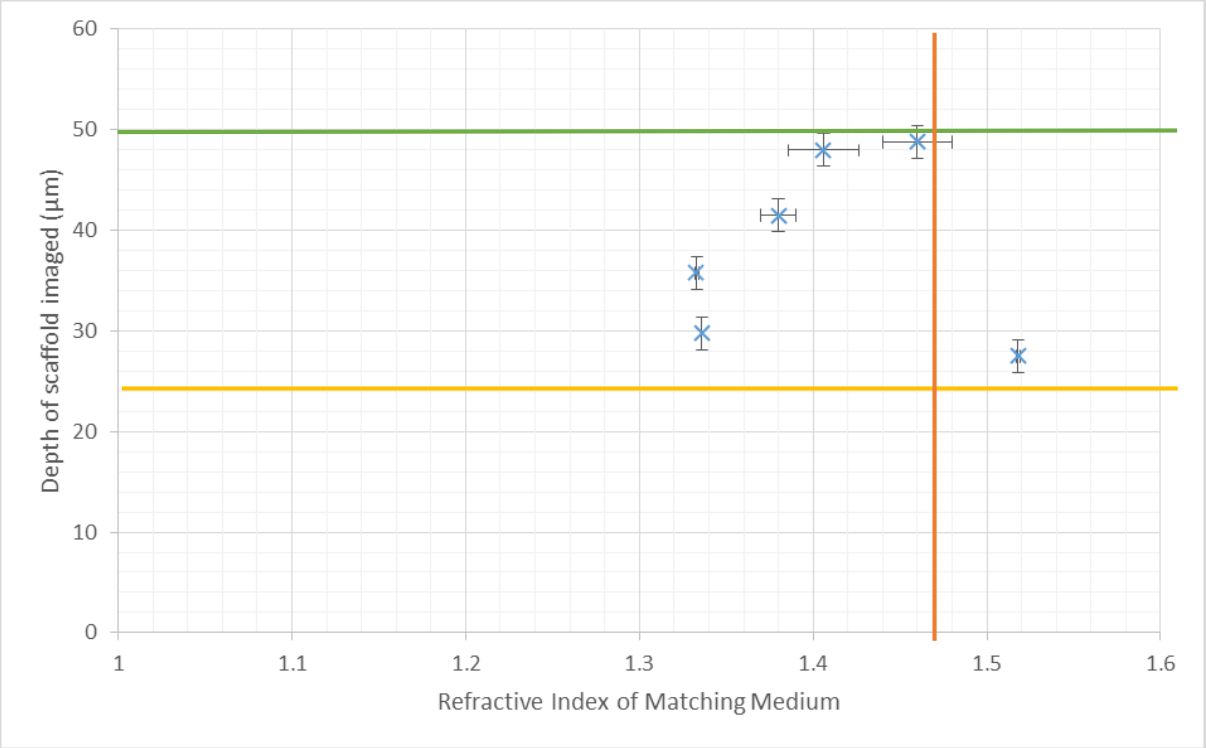

Figure **20** shows the relationship between the refractive index of the fluid used and the depth of the 4µm diameter fibre scaffold that was able to be imaged. The orange line indicates the refractive index of PLLA and the green line indicated the full depth of the scaffold (50µm). The yellow line indicates the depth of the scaffold which was able to be imaged when it was dry and free of any refractive index matching medium.

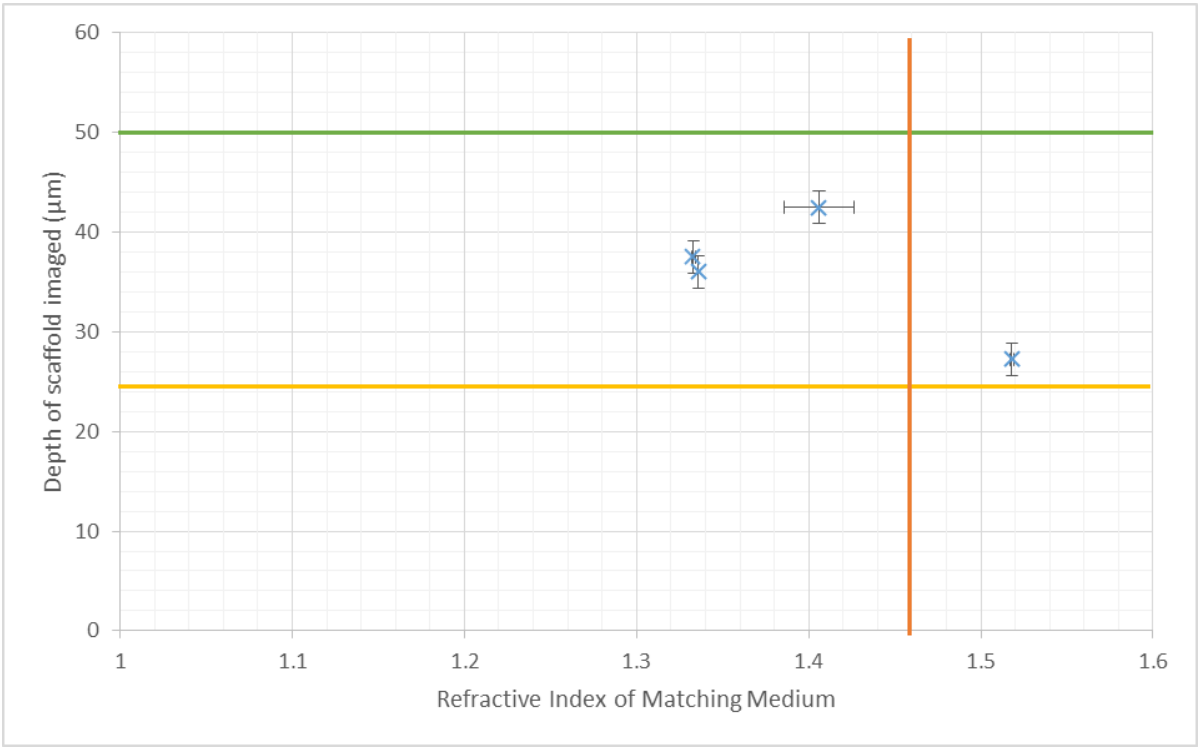

Figure **21** shows the relationship between the refractive index of the fluid used and the depth of the 1µm diameter fibre scaffold that was able to be imaged. The orange line indicates the refractive index of PLLA and the green line indicated the full depth of the scaffold (50µm). The yellow line indicates the depth of the scaffold which was able to be imaged when it was dry and free of any refractive index matching medium.

The graphs above shows the relationship between the refractive index of the fluid used and the depth of the scaffold that was able to be imaged. The orange line indicates the refractive index of PLLA and the green line indicated the full depth of the scaffold (50µm). The yellow line indicates the depth of the scaffold which was able to be imaged when it was dry and free of any refractive index matching medium. Despite varying levels of success with imaging depth, all media which allowed the scaffold to be imaged did show an increase in imaging depth. It is also clear to see that the imaging depth does indeed increase as the refractive index of the medium comes closer to the refractive index of the scaffolds. This corresponds with the predictions of the Fresnel equations governing refraction at media boundaries.

As seen in these tables and in Figures 20 and 21 the medium which improved the imaging depth most efficiently was 91% glycerol solution which was able to image to a depth of 48.8µm in the 4µm scaffolds.

4.2 Internal Structure of Scaffolds

By spending large amounts of time imaging a range of sections of different scaffolds, the project also yielded information on the internal structure of the Electrospinning Company's 1 and 4 µm fibre PLLA scaffolds. It was suspected but not confirmed that the fibres generally all lie parallel to the plane of the scaffold itself and this has been able to be confirmed using ImageJ and VolumeViewer. By using the "slice" function and looking at vertical slices through the scaffolds, it is possible to see the arrangement of the fibres vertically through the scaffolds. The scaffolds were also found to have long range isotropy over tens of micron ranges in the x-y plane as well as vertically.

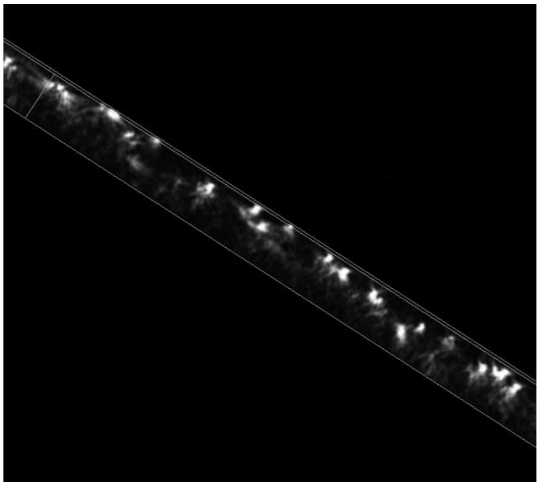

21 shows a slice taken through a 4µm diameter fibre scaffold using ImageJ and VolumeViewer

4.3 Intensity Measurements

The figures below were created using ImageJ function "Plot z-axis Profile" and Microsoft Excel. They show not only the depth of the scaffold imaged but the intensity of the images obtained. The initial

imaging of the dry scaffold is shown in black on both graphs. On the 4 µm diameter fibre scaffolds, a sharp increase in intensity can be seen in the 91% glycerol solution soaked sample. This could have been said to be due to reflection from the top layer of the glycerol solution. However, the intensity is not this high in the 55% glycerol solution sample. Therefore, it could be expected to be due to the close refractive index match of the 91% glycerol solution and the PLLA scaffolds. The oscillations in the intensity for the potassium iodide soaked sample are due to the salt crystals located in the top layer of the scaffold and highlights why this would not be a suitable matching medium for accurate measurements.

While the general trends remain similar for the 1 µm diameter fibre scaffold and the 4 µm diameter fibre scaffold, the results from the 1µm diameter fibre scaffold are generally less consistent and show discontinuities (in the case of the immersion oil sample). This could indicate some kind of issues with the matching media permeating in to the samples in the denser scaffolds.

.

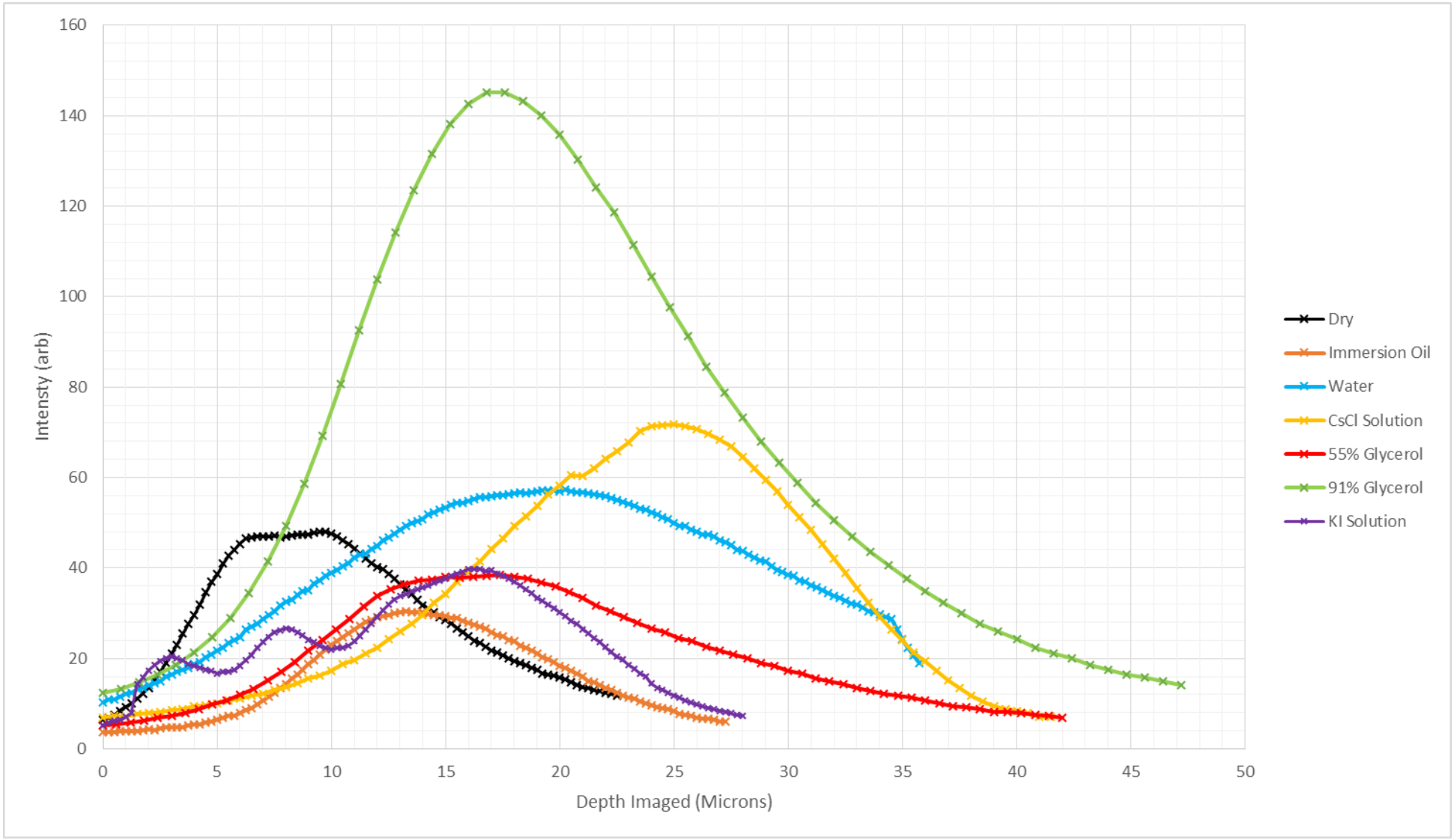

Figure **22** shows the intensity of the image slices through the depth of the 4µm fibre scaffold for the matching media used

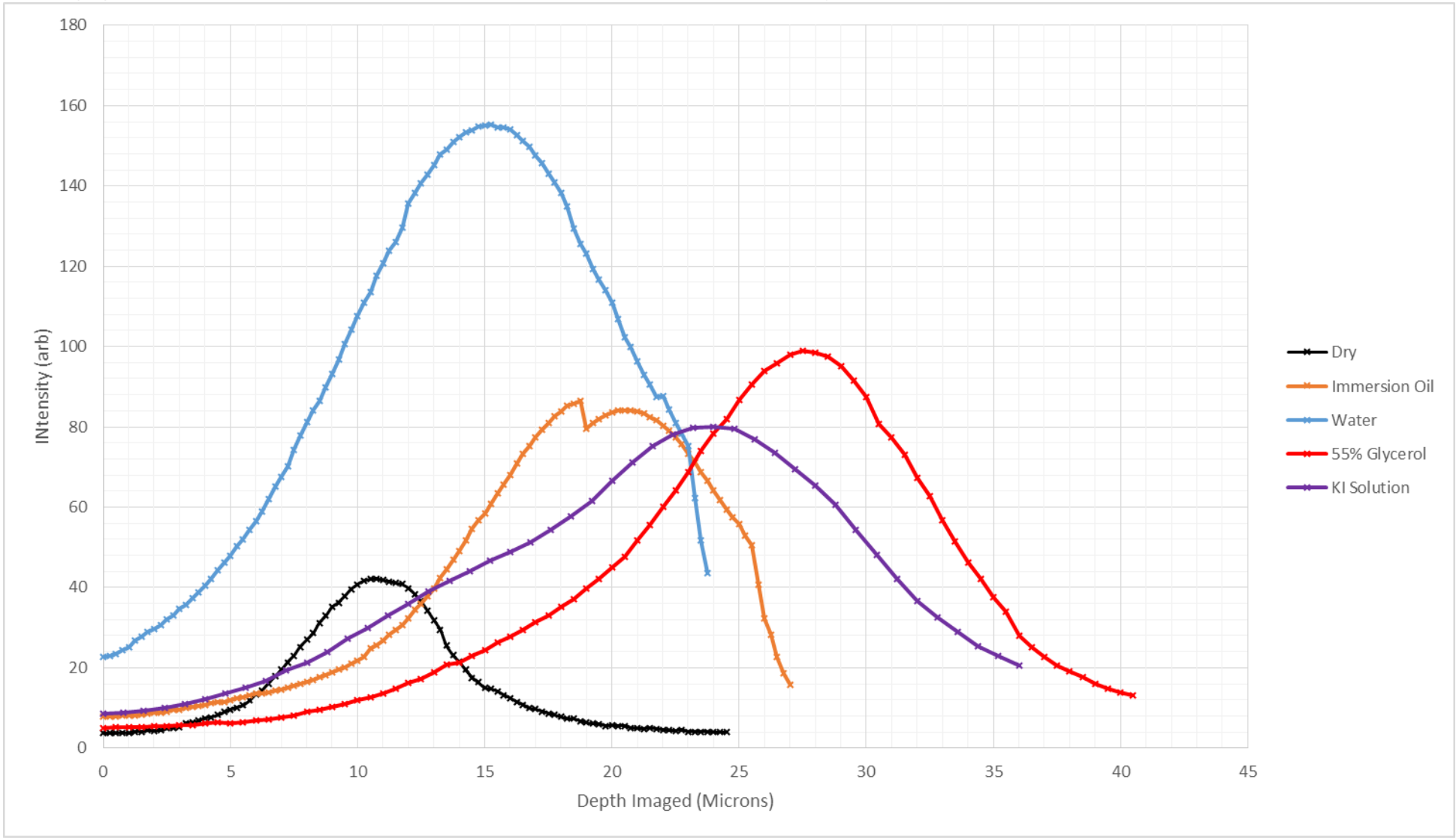

Figure **23** shows the intensity of the image slices through the depth of the 1µm fibre scaffold for the matching media used

5. Evaluation of Methodology

5.1 Depth Measurements

An important factor contributing to these results is assuming that the reported and measured value for the actual thickness of the scaffold is indeed 50 microns. It would be essential to confirm this value more rigorously before accepting the values given by refractive index matching as fact. There is evidence that the scaffolds may actually be thicker than this as when measuring the depth using the confocal microscope, this is actually the apparent depth as discussed in section 3.1.2. In theory, this should be less than the total depth of the scaffold by a factor of the refractive index of the matching medium. This could either indicate a discrepancy in the measured and reported values of the scaffolds or

5.2 Refractive Index Measurements

All of the refractive indices used in this project are based on reported values either from the manufacturer of the substance (in the case of the immersion oil) or on standard values for the refractive indices of solutions. This could have been measured for the specific solutions used using a refractometer and Snell's Law to calculate them. For the premixed solutions (including Caesium Chloride and Potassium Iodide) this would probably increase the uncertainty but for ones which have been mixed by hand specifically for this investigation, it would offer greater certainty of the refractive index.

5.3 Overall Quantization of Results

The project as a whole was largely qualitative and an investigation into overall trends and themes, while still being relatively quantitative. If the process of identifying the starting and ending points of the scaffolds could be effectively and efficiently quantised, this would add an additional level of certainty to the results. ImageJ could be used to find the mean intensity value for the images (as used in Figures 22 and 23) and use a single value of this for the starting and end points. However, this does not take in to account fully the drop in contrast and may not give the most accurate values.

5.4 Improving Versatility of Glycerol Imaging

In order to make the glycerol soaked imaging method as versatile as possible, it must be tested in other situations. Testing it on the 2μm diameter scaffolds would increase the number of situations where it would be a viable option. It would also be useful to test its effects on cells and imaging of biological samples more thoroughly. Scaffolds made from different materials will also have different optical and chemical properties and it would be necessary to investigate the usability of the method when using different scaffolds.

5.5 Potential Future Investigation

Even only considering the parameters of this project, there is still further investigation which could be carried out. There is an almost unlimited amount of liquids which could be trialled. It would be useful to investigate the permeation of fluids in to the scaffolds in a quantitative or qualitative manner. This could be further investigated by examining the effects of anionic, cationic, non-ionic surfactants on the scaffolds then applying the fluids as there may be residue or coating remaining on the scaffolds, although the electrospinning method is designed to avoid this. Organic compounds seem to have provided the most success in the investigation so far so it would be logical to continue with this investigation.

6. Conclusion

This was an open ended investigation and while significant work has been done in improving the imaging depth of confocal microscopy in electrospun PLLA scaffolds, there are still a huge amount of progress which could be made in this area, including but not limited to those outlined in section 5.5. The key success was that of glycerol as an imaging medium for PLLA scaffolds. It was effective to the point of doubling the volume of scaffold which was able to be imaged with only a small drop in contrast. It is also a widely available substance which is already used in the preparation of cell cultures for growth on electrospun scaffolds and therefore offers a relatively simple and easily implemented way to improve imaging of cell cultures grown within these scaffolds.

Acknowledgements

With huge thanks to Professor Ian Robinson, Dr Mohammed Yusuf, Deep Bhella, Neha Parmar, Graeme Robinson and everyone else at UCL and RCaH who has helped me so much throughout this project.

Bibliography

[1] S. G. Lipson, H. Lipson and D. S. Tannhauser, Optical Physics, Cambridge University Press, 1995.

[2] D. M. Shotton, "Confocal scanning optical microscopy and its applications for biological specimens," *Journal of Cell Science,* vol. 94, pp. 175-260, 1989.

[3] S. Inoue, "Foundations of Confocal Scanned Imaging in Light Microscopy," in *Handbook of Biological Confocal Microscopy (ed. James B Pawley)*, New York, NY, Plenum Press, 1989, p. 14.

[4] P. Torok and L. Mule'stagno, "Applications of scanning optical microscopy in materials science to detect bulk microdefects in semiconductors," *Journal of Microscopy,* vol. 188, no. 1, pp. 1-16, 1997.

[5] H. N. Chapman, "Microscopy: A new phase for X-ray imaging," *Nature,* vol. 476, pp. 409-410, 2010.

[6] T. Godden, R. Surman and M. J. Humphry, "Ptychographic microscope for three-dimensional imaging," *Optics Express,* vol. 22, no. 10, pp. 12513-12523, 2014.

[7] P. Hortola, "Generating 3D and 3D-like animations of a strongly uneven surface microareas of bloodstains from small series of partially out-of-focus digital SEM micrographs," *Micron,* vol. 41, no. 1, pp. 1-6, 2010.

[8] C. M. B. Goncalves, J. A. P. Coutinho and I. M. Marrucho, "Optical Properties: Refractive Index," in *Poly(Lactic Acid): Synthesis, Structures, Properties, Processing and Applications*, Hoboken, NJ, Wiley, 2010, p. 99.

[9] D. Li and Y. Xia, "Electrospinning of Nanofibers: Reinventing the Wheel?," *Advanced Materials,* vol. 16, no. 14, p. 1152, 2004.

[10] X. Zong, H. Bien and C.-Y. Chung, "Electrospun fine-textures scaffolds for heart tissue constructs," *Chemical Engineering and Processing: Process Intensification,* vol. 37, no. 3, pp. 257-263, 1998.

[11] S. J. Hollister, "Porous scaffold design for tissue engineering," *Nature Materials,* vol. 4, pp. 518-524, 2005.

[12] E. Guadalupe, D. Ramos, N. B. Shelke et. al., "Bioactive polymeric nanofiber matrices for skin regeneration," *Journal of Applied Polymer Science,* vol. 132, no. 16, 2015.

[13] M. Nakamura, M. Kobayashi et al., "Biocompatible Inkjet Printing Technique for Designed Seeding of Individual Living Cells," *Tissue Engineering,* vol. 11, no. 11-12, pp. 1658-1666, 2006.

[14] E. Hecht, "Light in Bulk Matter: Table 3.2 Maxwell's Relation: Gases at 0C and 1 atm," in *Optics*, San Francisco, CA, Pearson Educational, 2002, p. 66.

[15] E. Hecht, "Light in Bulk Matter: Table 3.2 Maxwell's Relation: Liquids at 20C," in *Optics*, San Francisco, CA, Pearson Educational, 2002, p. 66.

[16] United States Department of Agriculture, "U.S.D.A. Sucrose Conversion Table," Agriculture Marketing Service, U.S.D.A., Washington, DC, 1970.

[17] T. A. Scott, "Refractive Index of Ethanol-Water Mixtures and Density and Refractive Index of Ethanol-Water-Ethyl Ether Mixtures," *Journal of Physics Chemistry,* vol. 50, no. 5, pp. 406-412, 1946.

[18] A. Penzkofer, H. Glas and J. Schmailzl, "Optical Dispersion and Molar Refractivities of Alkali Halide Crystals and Aqueous Solutions," *Chemical Physics,* vol. 70, pp. 47-54, 1982.

[19] L. F. Hoyt, "New Table of the Refractive Index of Pure Glycerol at 20C," *Industrial and Engineering Chemistry,* vol. 26, no. 3, pp. 329-332, 1934.

[20] CRC , "Physical Constants of Organic Compounds," in *Handbook of Chemistry and Physics (ed. W. M. Haynes) 95th ed*, Boca Raton, FL, CRC Press, 2014, pp. 3-396.

[21] K. Thorn, C. Chamberlin and N. Tang, "Optimal clearing and mounting media for confocal microscopy of thick specimens," Nikon Imaging Centre at University of California, San Francisco , San Francisco, CA, 2011.

[22] National Institute of Health, "ImageJ - Image Processing and Analysis in Java," National Insitute of Health, [Online]. Available: http://imagej.nih.gov/ij/. [Accessed 17 March 2015].